Recurrent mutations of the exportin 1 gene (XPO1) and their impact on selective inhibitor of nuclear export compounds sensitivity in primary mediastinal B-cell lymphoma

Fabrice Jardin, A. Pujals, L. Pelletier, E. Bohers, V. Camus, S. Mareschal, S. Dubois, Brigitte Sola, Marlène Ochmann, F. Lemonnier, et al.

Recurrent mutations of the *exportin 1* gene (*XPO1*) and their impact on selective inhibitor of nuclear export compounds sensitivity in primary mediastinal B-cell lymphoma

Fabrice Jardin (1), Anais Pujals (2), Laura Pelletier (2), Elodie Bohers (1), Vincent Camus (1), Sylvain Mareschal (1), Sydney Dubois (1), Brigitte Sola (3), Marlène Ochmann (4), François Lemonnier (2), Pierre-Julien Viailly (1), Philippe Bertrand (1), Catherine Maingonnat (1) Alexandra Traverse-Glehen (4), Philippe Gaulard (2), Diane Damotte (6), Richard Delarue (7), Corinne Haioun (2), Christian Argueta (8),Yosef Landesman (8), Gilles Salles (5), Jean-Philippe Jais (9), Martin Figeac (10), Christiane Copie-Bergman (2), Thierry Jo Molina (11), Jean Michel Picquenot (1), Marie Cornic (1), Thierry Fest (4), Noel Milpied (12), Emilie Lemasle (1), Aspasia Stamatoullas (1), Peter Moeller (13), Martin J.S Dyer (14), Christer Sundstrom (15), Christian Bastard (1), Hervé Tilly (1), Karen Leroy (2).

- 1 Inserm U918, Centre Henri Becquerel, Rouen, France
- 2 Inserm U955 Team 09, APHP Hospital Henri Mondor, Créteil, France
- 3 Normandie Univ, UNICAEN, EA4652, Caen, France
- 4 Inserm U917, CHU Pontchaillou, Rennes, France
- 5 Hospices Civils de Lyon, Lyon-1 University, CNRS UMR5239, Pierre Benite, France
- 6 Department of Pathology, Hôpitaux Universitaires, Paris Centre, Team « Cancer, Immune Control, and Escape » INSERM U1138, Cordeliers Research Center
- 7 Department of Hematology, Necker Hospital, AP-HP; Paris, France
- 8 Karyopharm Therapeutics, Newton, MA 02459, United States of America
- 9 Department of Biostatistics, Hopital Necker, Paris, France
- 10 Functional Genomic Platforms, IRCL, Lille, France
- 11 Department of Pathology, Necker Hospital, AP-HP, Paris France
- 12 Department of Hematology, CHU de Bordeaux, France
- 13 Institute of Pathology, University of Ulm, Germany
- 14 Ernest and Helen Scott Haematological Research Institute, University of Leicester. Leicester,United Kingdom
- 15 Department of pathology, Uppsala, Sweden

Corresponding author: Fabrice Jardin, MD, PhD; e-mail address: fabrice.jardin@chb.unicancer.fr ; mailing address: UMR U918, Centre Henri Becquerel, 76000, Rouen, France; phone number:+3662905300; fax number: +33 23 20 82 555

Keywords: primary mediastinal B-cell lymphoma, exportin-1, targeted therapy

Running title: XPO1 mutations in primary mediastinal B-cell lymphoma

Abstract word count: 245**; Manuscript word count:** 4400

References: 53**; Number of Figures and Tables:** 4**; Number of Supplementary files:** 1

Abstract

Primary mediastinal B-cell lymphoma (PMBL) is an entity of B-cell lymphoma distinct from the other molecular subtypes of diffuse large B-cell lymphoma (DLBCL). We investigated the prevalence, specificity and clinical relevance of mutations of *XPO1*, which encodes a member of the karyopherin-β nuclear transporters, in a large cohort of PMBL. PMBL cases defined histologically or by gene expression profiling (GEP) were sequenced and the *XPO1* mutational status was correlated to genetic and clinical characteristics. The *XPO1* mutational status was also assessed in DLBCL, Hodgkin lymphoma (HL) and mediastinal gray-zone lymphoma (MGZL).The biological impact of the mutation on Selective Inhibitor of Nuclear Export (SINE) compounds (KPT-185/330) sensitivity was investigated *in vitro*. *XPO1* mutations were present in 28/117 (24%) PMBL cases and in 5/19 (26%) HL cases but absent/rare in MGZL (0/20) or DLBCL (3/197). A higher prevalence (50%) of the recurrent codon 571 variant (p.E571K) was observed in GEP-defined PMBL and was associated with shorter PFS. Age, International Prognostic Index and bulky mass were similar in XPO1 mutant and wild-type cases. KPT-185 induced a dose-dependent decrease in cell proliferation and increased cell-death in PMBL cell lines harboring wild type or *XPO1* E571K mutant alleles. Experiments in transfected U2OS cells further confirmed that the *XPO1* E571K mutation does not have a drastic impact on KPT-330 binding. To conclude the *XPO1* E571K mutation represents a genetic hallmark of the PMBL subtype and serves as a new relevant PMBL biomarker. SINE compounds appear active for both mutated and wild-type protein.

Introduction

Although diffuse large B-cell lymphoma (DLBCL) patients have greatly benefited from immunochemotherapy combinations in the past decade, between 30% and 40% of patients currently do not respond to treatment and rapidly relapse, emphasizing the need to understand the mechanisms involved and to identify predictive biomarkers. Primary mediastinal B-cell lymphoma (PMBL) is an entity of aggressive B-cell lymphoma that is clinically and biologically distinct from the other molecular subtypes of DLBCL, such as the germinal center B-cell-like (GCB) and activated B-cell-like (ABC) subtypes. PMBL-specific gene expression profiles have been reported, but in clinical practice, the diagnosis of PMBL remains essentially based on clinical, pathological and immunophenotypic characteristics that lack specificity[1, 2]. PMBL is thought to arise from thymic medullary B-cells and to manifest as an anterior mediastinal mass, predominantly in young women[3]. It is characterized by the constitutive activation of the Janus kinase-signal transducer and activator of transcription (JAK-STAT) signaling pathway[4]. Recently, RNA-Seq experiments identified somatic coding sequence mutations in PMBL[4]. PMBL mutations led to reduced phosphatase activity of the PTP1B protein, increasing the phosphorylation activity of the JAK-STAT pathway[5]. These mutations likely synergize with other known driver mutations reported in PMBL, including mutations in *SOCS1* and *STAT6*[4]. Of note, most of these genetic events are commonly shared with classical Hodgkin lymphoma (cHL). In contrast to GCB and ABC DLBCL, *EZH2*, *MYD88* and *CD79B* mutations or *BCL2/BCL6/MYC* rearrangements are typically absent from PMBL[6]. We recently detected a recurrent point mutation in the *XPO1* (*exportin 1*) gene (also referred to as *chromosome region maintenance 1; CRM1*), which results in the Glu571Lys (p.E571K) missense substitution, in refractory / relapsed (R/R) PMBL patients included in the LYSA (Lymphoma Study Association) LNH03 trial program[7, 8]. Exportin-1 (XPO1) is a member of the importin-β superfamily of nuclear export receptors (also termed karyopherins); this superfamily mediates the translocation of numerous RNAs and cellular regulatory proteins, including tumor suppressor proteins (TSPs) such as p53, BRCA1, survivin, NPM, APC, and FOXO. The hydrophobic groove of XPO1 binds to the leucine-rich nuclear export signal (NES) domain of its cargo proteins.

Missense substitutions targeting *XPO1* have previously been reported at a low frequency in chronic lymphocytic leukemia (CLL) and esophageal squamous cell carcinoma (ESCC), suggesting that these mutations may play a role in several oncogenic processes[9, 10]. A mutation had also been identified by RNA sequencing in one PMBL case[5]. In addition, cryptic *XPO1-MLLT10* translocations have been reported in T-cell acute lymphoblastic leukemia (T-ALL)[11]. Importantly, Selective Inhibitors of Nuclear Export (SINE) compounds, a new class of small molecule inhibitors, have been shown to effectively target XPO1 and retain TSPs in the nucleus. SINE are currently being

tested in phase 1 and 2 clinical trials for various cancer types[12, 13]. In this study, we investigated the prevalence, specificity, and biological and clinical relevance of *XPO1* mutations in PMBL cases and demonstrated that these mutations represent a new genetic hallmark of the PMBL subtype and cHL based on the rarity or absence of these mutations from GCB/ABC DLBCL or mediastinal gray-zone lymphoma (MGZL) cases.

Material and Methods

- Patients and tumor PMBL samples

To confirm and refine the preliminary results obtained via high-throughput targeted resequencing performed on the exploratory cohort [n = 215 patients enrolled in the LYSA LNH03 trial and translational research program, including 18 PMBL patients, referred to as molecularly defined PMBL cohort 1 (mPMBL1)][8], we extended the analysis to 99 additional PMBL patients, who were selected from three additional independent confirmatory cohorts. A detailed flow chart of the different series of patients is provided in Supplementary file 1. The second cohort [n = 14, referred to as molecularly defined PMBL cohort 2 (mPMBL2)] was defined according to gene expression profiling (GEP) as part of a previous study that established a PMBL signature[1]. Tumor DNA samples were provided by the Pathology Department of Henri Mondor Hospital and were obtained from patients treated between 1990 and 2001. The third cohort (n=38) included PMBL patients defined based on typical pathological and clinical criteria who were selected from a single institution between 2001 and 2014 (Henri Becquerel Center, Rouen, France); this cohort was referred to as monocentric histologically defined PMBL cohort 1 (hPMBL1). The fourth group, referred to as multicentric histologically defined PMBL cohort 2 (hPMBL2), included other PMBL cases enrolled in multicentric LNH03 LYSA program trials or in the 075 GOELAMS trial (hPMBL2)[14-18]. These cases were selected by experimented hematopathologists according to typical pathological and clinical criteria (n=47). Written informed consent was obtained from all participants at the time of enrollment for the patients included in the LYSA clinical trials.

- Hodgkin lymphoma samples and microdissection of HRS cells

To assess the frequency and specificity of the *XPO1* mutations, cases of cHL and MGZL, which are well-known to share several genetic features with PMBL, were analyzed. DNA samples were extracted from micro-dissected Reed-Sternberg (RS) cells of 19 cHL cases (including 7 nodular sclerosis cHL cases, 7 mixed cellularity cHL cases, 3 lymphocyte-rich cHL cases and 2 lymphocyte-depleted cHL cases).

HL cells were microdissected from 10-µm-thick sections frozen lymph node sections. RS cells were selected according to CD30 expression and were subsequently microdissected using a PALM

MicroBeam instrument (Zeiss, Germany) via the catapulting technique. Cells were catapulted (mean 300 cells per HL case) into lysis buffer and pooled. After capturing these cells, DNA extraction was performed using the AllPrep DNA Micro Kit (Qiagen, Netherlands). Pan-genomic amplification of extracted DNA was secondarily performed using the WGA4 Kit (Genomplex® Single Cell Whole Genome Amplification Kit, Sigma-Aldrich, St Louis, MO, USA) according to the manufacturer's recommendations.

Twenty cases of MGZL were selected from a single institution (Hospices Civils de Lyon, France) and reviewed by a panel of expert pathologists, based on morphologic and phenotypic characteristics intermediate between cHL and PMBL as previously described[19]. 14 cases had a predominant HL-like morphology, 3 cases had a predominant PMBL-like morphology, 2 cases were considered as composite and 1 case unclassified.

- Cell lines

The previously described PMBL-derived cell lines MedB-1, Karpas1106 and U-2940 were kindly provided by Peter Möller (University of Ulm, Germany), Martin Dyer (University of Leicester, United Kingdom) and Christopher Sundström (University of Uppsala, Sweden), respectively[20-22]. The Jurkat T-ALL cell line was used as a control in some experiments. The cell lines were cultured at 37˚C in a 5% CO_2 atmosphere in either Iscove medium (Iscove's Modified Dulbecco's Medium, Gibco®, Life Technologies™) (MedB-1 and Karpas1106) or RPMI medium (U-2940 and Jurkat) supplemented with 20% (Karpas1106, MedB-1 and U-2940) or 10% (Jurkat) fetal calf serum (ID Bio®), 2 mM L-glutamine (Gibco®, Life Technologies™), 100 U/ml penicillin, 100 µg/ml streptomycin (Gibco®, Life Technologies™), non-essential amino acids (Gibco®, Life Technologies™) (MedB1 and Karpas1106) and 1 mM sodium pyruvate (Gibco®, Life Technologies™) (Jurkat).

- *XPO1* sequencing experiments

DNA was extracted from frozen or FFPE tumor biopsy samples using standard methods. The patients in mPMBL1 were sequenced using NGS technology (PGM); these results were reported elsewhere (Dubois et al., submitted). For the other cohorts, standard Sanger sequencing was performed after PCR amplification using the following primers: DNA extracted from frozen tissues: XPO1-ex15F: GCAATGCATGAAGAGGACG; XPO1-ex15R: TCATTTATTTTGTCCTGGACTCC; DNA extracted from FFPE tissues: XPO1-ex15FFPE-F: TATGTGAACAGAAAAGAGGCAAAG; XPO1-ex15FFPE-R: AAAGAAAGAGATTTACCATGCATG; XPO1-ex15FFPE-F2: CTCACTGGAAATTTCTGAAGACTGTAG; XPO1-ex15FFPE-R2: TCATTTATTTTGTCCTGGACTCC. To improve the sensibility of *XPO1* mutation detection in cHL and MGZL, we designed a dedicated *XPO1* digital PCR (dPCR) assay (for details of the assay, see supplementary file and [23]).

- Comparative genomic hybridization (CGH) arrays

To assess the *XPO1* copy number, CGH was performed on 208 DLBCL biopsies and a normal commercial DNA pool (Promega, Mannheim, Germany) using 4x180K SurePrint G3 Human CGH microarrays (Agilent, Santa Clara, CA). Primary analysis was performed using Feature Extractor (10.5.1.1); probe-level signals were segmented using the CBS algorithm ("DNAcopy" R package, version 1.36.0); and copy number variations (CNVs) were called using sample-specific log-ratio thresholds accounting for the estimated cellularity of the samples. The resulting copy number data were queried and visualized using Rgb[24].

- Gene expression profiling (GEP)

Patients were classified into the GCB, ABC, PMBL and "other" (unclassified) subtypes based on published signatures using HGU133 Plus2.0 Affymetrix GeneChip arrays (Affymetrix) (Supplementary Methods). A single probe set was selected to represent the expression of each gene of interest based on JetSet "best" probe set selection (version 2.14.0)[25]. *XPO1*-based comparative expression analysis was performed using LIMMA to model the expression of 15 262 probe sets according to the *XPO1* mutation and binary amplification status[26]. A single probe set was selected to represent the expression of each gene of interest (including *XPO1*) based on JetSet "best" probe set selection (version 2.14.0)[25]. Only JetSet "best" probe sets displaying a minimal mean expression and variance of 3.5 and 0.05, respectively, were considered for this task.

- Cell proliferation assays

The SINE compound, KPT-185 was provided by Karyopharm Therapeutics (Newton, MA, United States of America). Cells were seeded in 96-well plates and treated for 24, 48 or 72 hours with KPT-185 at concentrations ranging from 10 nM to 2000 nM. The inhibition of cell growth induced by KPT-185 in PMBL cell lines was assessed using an MTS assay (CellTiter 96 Aqueous Non-Radioactive Cell Proliferation Assay, Promega) according to the manufacturer's protocol. The calculation of the KPT-185 IC50 at 72 h was determined using GraphPad Prism software (GraphPad Software, La Jolla, CA, United States of America) using the dose-response variable slope model. The cell proliferation indicator dye eFluor® 670 (eBioscience, San Diego, United States of America) was used to monitor cell division during KPT-185 exposure. This fluorescent dye binds to any cellular protein containing primary amines, and as cells divide, the dye is distributed equally between daughter cells, which can be detected as the successive halving of the fluorescence intensity of the dye. Cells were incubated in DMSO or 2 µM KPT-185 for 48 h and analyzed via flow cytometry using a CyAn™ ADP Analyser flow cytometer (Beckman Coulter) following fixation with 2% paraformaldehyde.

- Apoptosis assay

Cells were harvested after 20 hours of exposure to DMSO or 2 µM KPT-185, washed twice with phosphate-buffered saline, resuspended in Annexin buffer (10 mM HEPES/NaOH (pH 7.4), 140 mM NaCl, and 55 mM CaCl2) supplemented with 2.5 µg/ml FITC-labeled Annexin-V (Roche Applied Science, Meylan, France) and incubated at room temperature for 10 minutes. The cells were then washed, resuspended in Annexin buffer supplemented with propidium iodide (3 µg/ml) and analyzed via flow cytometry using a CyAn™ ADP Analyser flow cytometer (Beckman Coulter).

- Transfection of REV-GFP expressing U2OS cells with plasmids encoding XPO1 variants

Osteosarcoma U2OS cells, which stably express the fluorescently labelled XPO1 cargo viral protein REV-GFP[27], were transiently transfected with expression plasmids encoding wild type or E571 mutant XPO1 proteins coupled to a red fluorescent tag. Cells were treated with the clinical SINE compound selinexor (KPT-330, Karyopharm therapeutics) and nuclear localization of REV-GFP and XPO1 was analyzed in transfected cells by confocal microscopy.

- Western blot and immunohistochemistry

Western blot analysis of XPO1 expression was performed according to a standard protocol. First, 10 µg of whole-cell protein extracts were loaded on a precast 4–20% Mini-PROTEAN® TGX™ Gel (Bio-Rad, Hercules, CA, United States of America). After electrophoresis, the proteins were transferred to PVDF membranes (Immobilon-P, Merck Millipore, Billerica, MA, United States of America), which were then probed with antibodies specific for XPO1 (Santa Cruz Biotechnology, Santa Cruz, CA, United States of America) or β-actin (1/10 000, Sigma). The methods used for immunocytochemistry and immunohistochemistry are indicated in **Supplementary file**.

- Statistical analysis

Tumor responses after induction therapy and at the end of treatment were classified as complete response (CR), unconfirmed complete response (CRu), partial response (PR), stable disease (SD) or progressive disease (PD) based on the International Workshop 1999 Cheson criteria[28]. Progression-free survival (PFS) was calculated from the date of enrollment to the date of disease progression, relapse, re-treatment or death from any cause. Overall survival was calculated from the date of enrollment or the date of diagnosis to the date of death from any cause. Survival was estimated using the Kaplan-Meier product limit method, and the results were compared using the log-rank test. A Fisher exact-test was used to assess the associations between the *XPO1* genotype and patient characteristics.

Results

- ***XPO1* mutations are highly specific for the PBML subtype and are located in the NES-binding domain**

Targeted sequencing of a dedicated gene panel in an exploratory cohort of 215 lymphoma cases identified that 7 of the 18 cases in the mPMBL1 cohort harbored *XPO1* mutations. We confirmed the presence of recurrent *XPO1* mutations in the three additional cohorts analyzed. *XPO1* mutations were observed in 9/14 (64%) cases in mPMBL2 and at a lower frequency in the two hPMBL groups [6/38 cases (16%) and 6/47 cases (13%) in hPMBL1 and hPMBL2, respectively]. Overall, *XPO1* mutations were detected in 28/117 PMBL cases (24.5%) (**figure 1**). The highly recurrent E571K variant (27/28 mutations, NM_003400, chr2:g.61719472C>T) is located within the Heat repeat domain H12A, which constitutes a hydrophobic site (NES Cleft) crucial for XPO1 cargo function (**figure 1**)[13, 29]. In addition, an alternative variant (R553P) was observed in 1 PMBL case (**supplementary table 1**). The pathogenicity of the E571K mutation was predicted using three different algorithms (SIFT score = 0.02; PolyPhen score =1; MutationTaster score =1)[30, 31]. In the two cases analyzed by WES, we confirmed that the E571K mutation was acquired (GHE0536 19/66 reads as compared to 0/89 reads in normal matched DNA, tumor purity estimation =55%; GHE0609 8/57 reads versus 0/64 reads in normal matched DNA, tumor purity estimation =35%, supplementary data[7]). By targeted resequencing using the PGM platform the variant allele frequency range was 7.32%-24.24% (median 16.72%).

Among DLBCL cases, an E571G variant was detected in a single GCB (1/83) case, and two E571K variants were detected in 1/81 ABC case and 1/33 “other” (unclassified) case (**Supplementary table 1**). The E571K mutation was observed in 1/19 RS micro-dissected HL case (scleronodular type) using Sanger sequencing and in 4/19 additional cases (2 mixed cellularity, 1 lymphocyte depleted, 1 lymphocyte rich) by dPCR (26% of mutated cHL overall). No mutation was detected in 0/20 MGZL cases by Sanger sequencing or dPCR (**figure 1**).

Importantly, the E571K variant was detected as a heterozygous mutation in MedB-1, a PMBL-derived cell line, whereas the two other PMBL cell lines tested, Karpas1106 and U-2940, did not display any variants in *XPO1* exon 15.

- ***XPO1* mutations, CNV and GEP**

XPO1 is located on chromosome 2p15 near the c-REL 2p16.1 locus; well-known for gains or amplifications in PMBL, GCB-DLBCL and cHL[3, 32-35]. In the 20 PMBL cases analyzed via CGH, copy number gains in the *XPO1* locus were observed in 8 cases (40%, ranging from 3 to 7 copies, **Supplementary Figure 1A**); this rate was higher than that observed for ABC DLBCL (8/70, 11%) but similar to that observed for GCB DLBCL (21/74, 28%). A significant correlation was observed between the *XPO1* copy number and the expression of the corresponding mRNA, suggesting a gene

dosage effect (p=0.00106, Mann-Whitney test). In contrast, we did not observe any correlation between the *XPO1* mutation status and the level of *XPO1* mRNA expression (**Supplementary Figure 1A**). There was no significant difference in the level of *XPO1* mRNA expression between the PMBL, ABC and GCB subtypes (**Supplementary Figure 1B**). In all PMBL cases, *XPO1* gene copy gains were associated with REL copy gains, and in all but one DLBCL case (**Supplementary Figure 1C**). One case (GHE1287) displayed an *XPO1* mutation, 7 copies of the gene and 11 copies of *REL*. Overall 13/18 PMBL cases (72%) display either copy gains and/or *XPO1* mutations. Of note, MedB-1 and Karpas1106 cells are also known to display 2p16 copy number gains[33].

We then compared GEPs of mutated and wild-type *XPO1* patients using a multivariate model including the amplification status. We observed a significantly higher level of expression of several genes (FDR < 0.1), including *PARP15*, in PMBL cases harboring *XPO1* mutations compared to PMBL cases harboring wild-type *XPO1* (**Supplementary Figure 1C and supplementary table 2**). Interestingly, PARP-15 (also referred to as ARTD7 or BAL3) is a nuclear protein containing N-terminal macro domains and displaying C-terminal poly(ADP-ribose) polymerase (PARP) activity, which was originally reported in refractory/aggressive B-cell lymphoma[36]. The list of probes differentially expressed was significantly enriched in genes containing regulatory motifs dependent on transcription factor 3 (TCF3, E2A immunoglobulin enhancer binding factors E12/E47) (gene set enrichment analysis, p-value $=10^{-10}$, FDR q value $=10^{-6}$) (**Supplementary table 2**).

- **Functional characterization of PMBL cell lines carrying WT or mutant XPO1.**

To assess the biological impact of the E571K variant on SINE compound sensitivity, we evaluated the effects of KPT-185, a SINE compound, on PMBL cell lines and compared the results to those described for Jurkat T-ALL cells, which are known to be highly sensitive to this compound[12, 37]. XPO1 expression in the PMBL and Jurkat cell lines was assessed via Western blot. As previously described, SINE compound exposure induced the downregulation of XPO1 expression in all cell lines (**figure 2A**)[38]. XPO1 immunocytochemistry revealed strongly intense nuclear staining in all cell lines (dilution 1/50), with no difference between the PMBL cell lines carrying WT (Karpas 1106 and U2940) and mutant XPO1 (MedB-1) (**supplementary figure 2**). Nuclear staining for XPO1 was confirmed via immunohistochemistry of 4 XPO1 mutant and 10 XPO1 WT PMBL cases (**supplementary figure 2**). KPT-185 dose-dependently inhibited cell proliferation in all cell lines (**Figure 2B and supplementary figure 3**) and displayed higher cytotoxicity to the Jurkat cell line (IC_{50}=106 nM) than to the PMBL cell lines (U-2940 IC_{50} = 393 nM, Karpas1106 IC_{50} = 523 nM, MedB-1 IC_{50} = 680 nM); MedB-1 cells were the least responsive to this drug. Labeling of the cells with the cell proliferation indicator dye eFluor 670 showed that 2 μM KPT-185 significantly inhibited PMBL cell division (**Figure 3C**), although to a lesser extent in MedB-1 cells (**Figure 2D**). Treatment with 2 μM KPT-185 for 20 hours strongly induced apoptosis in Jurkat cells (72% Annexin V-positive

cells), whereas apoptosis induction was moderate in U-2940 and Karpas1106 cells (37% and 32% Annexin V-positive cells, respectively) and was weak in MedB-1 cells (11% Annexin V-positive cells) (**Figure 3E)**. Taken together, these results show that PMBL cell lines are sensitive to the SINE compound. The MedB-1 cell line, which carries a heterozygous *XPO1* E571K mutation, displayed a slightly weaker response to KPT-185 than the Karpas1106 and U-2940 cell lines but remains responsive to this drug, with an EC50 comparable to that for the other PMBL cell lines and on the same order of magnitude as the EC50 for CLL cells[13].

In keeping with these results, the E571 mutated XPO1 proteins were inhibited by Selinexor in U2OS cells. KPT-330 Treatment inhibited the nuclear export of REV-GFP similarly in cells expressing wild-type and E571 mutated XPO1 protein. By contrast, when XPO1 cysteine 528 was mutated to serine, the ability of selinexor to bind covalently to XPO1 was prevented and therefore nuclear export was not blocked **(Figure 3).**

- **Clinical relevance of *XPO1* mutations for PMBL**

Considering the frequency of *XPO1* mutations, the clinical relevance and prognostic impact of *XPO1* mutations was assessed independently in mPMBL and hPMBL cohorts. The main clinical features, including age, gender, age-adjusted IPI (aaIPI), IPI, the LDH level and bulky mass (> 10 cm), appeared to be similar between the *XPO1* mutant and WT patients in both the hPMBL and mPMBL groups (**Table 1**). In the total population (n = 117), we observed a preferential female distribution of XPO1 mutations [19/56 (34%) compared to 9/61 (15%) in male patients; p =0.02, Fisher exact test] (**Supplementary table 3**).

The mPMBL and hPMBL patients were similar with respect to gender, age, LDH level, IPI/aaIPI, and bulky mass (supplementary table 3) but were treated heterogeneously, including more frequent rituximab usage in hPMBL patients (76/85, 89%) than in mPMBL patients (15/32, 47%) ($p < 0.001$). Conversely, ACVBP and ACVBP-like regimens were used more frequently in the mPMBL cohort ($p = 0.006$) (**Supplementary table 3**).

Based on a median follow-up duration of 42 months, *XPO1* mutant patients exhibited significantly decreased PFS (3y PFS = 74% [CI95% 55-100]) compared to wild-type patients (3y PFS = 94% [CI95% 83-100], log-rank test p=0.049) and a trend toward decreased OS (3y OS = 56% [CI95% 36-87] vs. 3y OS = 88% [CI95% 73-100], log-rank test p=0.067) in the mPMBL cohort (n = 32) (**Supplementary Figures 4A and 4C**). In contrast, based on a median follow-up duration of 37 months, we did not observe any prognostic impact of the *XPO1* mutation status in the hPMBL cohort (**Supplementary Figures 4B and 4D**).

Details regarding clinical features, treatments and chemotherapy regimens for the 31 *XPO1* mutant cases (including the 28 PMBL cases and the 3 non-PMBL DLBCL cases) are presented in **Supplementary table 1**. The level of *XPO1* mRNA expression as assessed by GEP did not correlate with OS or PFS in the mPMBL1 cohort (data not shown).

Discussion

In the present work, we demonstrate for the first time the high prevalence of a recurrent SNV of *XPO1* in PMBL but also in cHL. This mutation was observed in approximately 25% of cases and appeared to be a specific genetic feature of this subtype, as this mutation was observed at a very low frequency or absent from MGZL and GCB/ABC DLBCL cases. WES-based experiments of sorted RS cells recently identified new point mutations in cHL cases, including several mutations already reported in PMBL, such as *CIITA*, *SOCS1*, *STAT6* and *B2M* mutations, as well as one case harboring the E571K *XPO1* mutation [33, 39, 40]. The *XPO1* mutation appears to serve as a distinctive genetic feature that facilitates the differential diagnosis of PMBL from DLBCL with mediastinal involvement, or MGZL, which are genetically similar but clearly distinct in their natural history and outcome[41, 42]. Our data enrich the complex genomic landscape and genetic particularity of the PMBL entity, as recently highlighted by a study that used RNAseq and WGS approaches[5].

In contrast to *XPO1* mutations, gains at the chromosome 2p16.1-2p15 locus, which contains both the *REL* and *XPO1* genes, were commonly observed in GCB DLBCL, cHL and PMBL cases[33-35]. However, only the putative effect of such gains on c-REL expression and the resulting alterations in the NFKB pathway have been deeply investigated[43]. The frequent genomic overrepresentation of *REL* in PMBL does not necessarily correlate with NFKB activation, suggesting that the growth advantage related to 2p16.1-15 gains could be related to other candidate genes, such as *BCL11A* and *XPO1*[35].

Despite similar clinical features between the two cohorts, the rate of *XPO1* mutations strongly differed between hPMBL and mPMBL (13% and 64%, respectively). These contrasting results most likely highlight the difficulty in distinguishing “true” PMBL from other subtypes of DLBCL with mediastinal involvement, as initially reported by Rosenwald et al., who established a molecular signature of PMBL[1]. A recent study identified GEP-defined PMBL without any mediastinal involvement, suggesting that GEP definition and genotype are more effective to delineate this entity than anatomical and histopathological criteria[44]. Therefore, *XPO1* mutations, in combination with other recurrent reported SNVs and GEP results, contribute to the more accurate elucidation of the molecular basis of this lymphoma subtype.

The functional relevance of the E571K variant is currently unknown. Preliminary structural analysis suggests that E571 mutations likely affect cargo NES binding and may change the open-closed

equilibrium of the hydrophobic groove of XPO1. For instance, the E571-K568 salt bridge, which has been observed in every XPO1 structure, sits at the narrowest part of the NES groove and is likely important for groove shape (unpublished data courtesy of Dr. Chook, University of Texas). Most of the reported genetic alterations in PMBL, including *JAK2* gains and *STAT6*, *SOCS1* or *PTPN1* mutations, coincide and synergize to activate the JAK-STAT6 pathway[39, 45]. XPO1 is known to be involved in the nucleo-cytoplasmic export of STAT1, which is also known to be highly expressed in PMBL; therefore, XPO1 may contribute to the tuning of the JAK-STAT pathway[2, 46]. Other proteins known to play an important role in PMBL pathophysiology, including CIITA, IKBKB and FOXO1, are also under the control of XPO1 cargo function [47-50]. Interestingly, mathematical modeling of XPO1 inhibitor target pathways based on protein-protein interaction network analysis in cells treated with XPO1 inhibitors suggested that the combination of JAK-STAT inhibitors with XPO1 inhibitors may enhance efficacy against JAK-STAT-driven tumors[51, 52]. *STAT6* mutations are highly recurrent in PMBL and are not mutually exclusive with *XPO1* variants (8/16 *XPO1* mutant cases displayed *STAT6* mutations in the mPMBL cohort; Dubois et al, submitted, and K Leroy et al, personal data). We hypothesize that *XPO1* mutations may play an important role in PMBL physiopathology by interacting with phospho-STAT6 or other phospho-STAT nucleo-cytoplasmic shuttling and may act synergistically with several other genetic changes to contribute to the deregulation of the JAK/STAT axis.

Importantly, E571 is located in a highly charged region of the NES groove, which surrounds cysteine residue 528 (C528), known to be the conjugation site of KPT-185/KPT-330/LMB[53]. Therefore, mutations in E571 may also affect the rates of conjugation and deconjugation of these molecules. However, our results indicate that the inhibition of XPO1 by KPT-185 / KPT-330 is cytotoxic to all PMBL cell lines and effective in *XPO1* mutant transfected U2OS cells, suggesting no major impact of the E571 variant in SINE compounds efficacy.

The differential GEP observed between the XPO1 mutant and WT PMBL cases, including a higher expression level of PARP15/BAL3 and several genes controlled by TCF3, strongly suggests a functional impact of XPO1 mutations [46].

Increased XPO1 expression has been associated with poor prognosis in MCL and ovarian cancer patients and has been detected in several other cancers such as glioma, osteosarcoma, and pancreatic and cervical cancer[54, 55]. In CLL, the prognostic value of *XPO1* mutations is unclear [9]. Based on our study, the prognostic impact of *XPO1* mutations on PMBL is also uncertain. In the mPMBL cohort, XPO1 mutations were highly prevalent (50%) and were observed in unusual relapsing or refractory cases; these results contrasted with the absence of an impact of these mutations on the hPMBL cohort. The more frequent rituximab usage in hPMBL patients (76/85, 89%) than in mPMBL patients (15/32, 47%), as well as a fivefold lower mutation rate in hPMBL than in mPMBL, may

explain these inconclusive results regarding the prognostic impact of *XPO1* mutations. Furthermore, the proportion of patients who received adjuvant radiotherapy was different between mutated (3.5%) and unmutated patients (9%) and may have played a role in reducing the number of progressions in this group. However, one could hypothesize that in rare PMBL cases, *XPO1* mutations may synergize with additional genetic events to favor chemotherapy resistance.

In conclusion, although the oncogenic properties of *XPO1* mutations remain to be determined, their recurrent selection in PMBL and cHL strongly supports their involvement in the pathogenesis of these diseases.

- Funding: This work was supported by the French National Institute of Cancer (INCA) and the Cancer Research Association (ARC), the Ligue regionale contre le cancer (Normandie).
- Acknowledgments: The authors thank Dr. Lin Chook for her critical review and for providing the molecular data on the conformation of XPO1/CRM1 protein residues.

- Authors' contributions:

- LYSA clinical trial investigators: RD, NM, GS, CH, HT, NM, and TF
- Pathologic review and case selection: JMP, DD; ATG, TJM, FL, MO, and PG
- NGS and PCR experiments and Sanger sequencing: EB, VC, CM, SD, and PB
- CGH and GEP experiments: MF, SM; JPJ, and MF
- Statistical analysis: SM, JPJ; and PJV
- Cell experiments: LP, AP, YL, MD, PM, CS, BS, CA and KL
- Bioinformatics analysis: SM; and JPJ
- Immunohistochemistry: JMP, MC, and VC
- Clinical data collection: VC, FJ, HT, FL, and MO
- Microdissection experiments: EL, AS, CB, and JMP
- Supervision and study design: FJ and KL

Conflict of interest

Yosef Landesman is an employee of Karyopharm Therapeutics.

References

1. Rosenwald A, Wright G, Leroy K, et al. Molecular diagnosis of primary mediastinal B cell lymphoma identifies a clinically favorable subgroup of diffuse large B cell lymphoma related to Hodgkin lymphoma. J Exp Med 2003;198:851-862.

2. Savage KJ, Monti S, Kutok JL, et al. The molecular signature of mediastinal large B-cell lymphoma differs from that of other diffuse large B-cell lymphomas and shares features with classical Hodgkin lymphoma. Blood 2003;102:3871-3879.
3. Dunleavy K, Wilson WH. Primary mediastinal B-cell lymphoma and mediastinal gray zone lymphoma: do they require a unique therapeutic approach? Blood 2015;125:33-39.
4. Steidl C, Gascoyne RD. The molecular pathogenesis of primary mediastinal large B-cell lymphoma. Blood 2011;118:2659-2669.
5. Gunawardana J, Chan FC, Telenius A, et al. Recurrent somatic mutations of PTPN1 in primary mediastinal B cell lymphoma and Hodgkin lymphoma. Nature genetics 2014;46:329-335.
6. Gebauer N, Hardel TT, Gebauer J, et al. Activating mutations affecting the NF-kappa B pathway and EZH2-mediated epigenetic regulation are rare events in primary mediastinal large B-cell lymphoma. Anticancer research 2014;34:5503-5507.
7. Mareschal S, Dubois S, Viailly P, et al. Whole Exome Sequencing of Relapsed/Refractory Patients Expands the Repertoire of Somatic Mutations in Diffuse Large B-Cell Lymphoma. Genes chromosomes and cancer 2015:in press.
8. Dubois S, Viailly PJ, Mareschal S, et al. Next Generation Sequencing in Diffuse Large B Cell Lymphoma Highlights Molecular Divergence and Therapeutic Opportunities: a LYSA Study. Clinical cancer research : an official journal of the American Association for Cancer Research 2016.
9. Jeromin S, Weissmann S, Haferlach C, et al. SF3B1 mutations correlated to cytogenetics and mutations in NOTCH1, FBXW7, MYD88, XPO1 and TP53 in 1160 untreated CLL patients. Leukemia 2014;28:108-117.
10. Lin DC, Hao JJ, Nagata Y, et al. Genomic and molecular characterization of esophageal squamous cell carcinoma. Nature genetics 2014;46:467-473.
11. Bond J, Bergon A, Durand A, et al. Cryptic XPO1-MLLT10 translocation is associated with HOXA locus deregulation in T-ALL. Blood 2014;124:3023-3025.
12. Etchin J, Sanda T, Mansour MR, et al. KPT-330 inhibitor of CRM1 (XPO1)-mediated nuclear export has selective anti-leukaemic activity in preclinical models of T-cell acute lymphoblastic leukaemia and acute myeloid leukaemia. British journal of haematology 2013;161:117-127.
13. Lapalombella R, Sun Q, Williams K, et al. Selective inhibitors of nuclear export show that CRM1/XPO1 is a target in chronic lymphocytic leukemia. Blood 2012;120:4621-4634.
14. Peyrade F, Jardin F, Thieblemont C, et al. Attenuated immunochemotherapy regimen (R-miniCHOP) in elderly patients older than 80 years with diffuse large B-cell lymphoma: a multicentre, single-arm, phase 2 trial. The Lancet Oncology 2011;12:460-468.
15. Recher C, Coiffier B, Haioun C, et al. Intensified chemotherapy with ACVBP plus rituximab versus standard CHOP plus rituximab for the treatment of diffuse large B-cell lymphoma (LNH03-2B): an open-label randomised phase 3 trial. Lancet 2011;378:1858-1867.
16. Delarue R, Tilly H, Mounier N, et al. Dose-dense rituximab-CHOP compared with standard rituximab-CHOP in elderly patients with diffuse large B-cell lymphoma (the LNH03-6B study): a randomised phase 3 trial. The Lancet Oncology 2013;14:525-533.
17. Fitoussi O, Belhadj K, Mounier N, et al. Survival impact of rituximab combined with ACVBP and upfront consolidation autotransplantation in high-risk diffuse large B-cell lymphoma for GELA. Haematologica 2011;96:1136-1143.
18. Ketterer N, Coiffier B, Thieblemont C, et al. Phase III study of ACVBP versus ACVBP plus rituximab for patients with localized low-risk diffuse large B-cell lymphoma (LNH03-1B). Annals of oncology : official journal of the European Society for Medical Oncology / ESMO 2013;24:1032-1037.
19. Traverse-Glehen A, Pittaluga S, Gaulard P, et al. Mediastinal gray zone lymphoma: the missing link between classic Hodgkin's lymphoma and mediastinal large B-cell lymphoma. The American journal of surgical pathology 2005;29:1411-1421.
20. Moller P, Bruderlein S, Strater J, et al. MedB-1, a human tumor cell line derived from a primary mediastinal large B-cell lymphoma. International journal of cancer Journal international du cancer 2001;92:348-353.

21. Nacheva E, Dyer MJ, Metivier C, et al. B-cell non-Hodgkin's lymphoma cell line (Karpas 1106) with complex translocation involving 18q21.3 but lacking BCL2 rearrangement and expression. Blood 1994;84:3422-3428.
22. Sambade C, Berglund M, Lagercrantz S, et al. U-2940, a human B-cell line derived from a diffuse large cell lymphoma sequential to Hodgkin lymphoma. International journal of cancer Journal international du cancer 2006;118:555-563.
23. Camus V, Sarafan-Vasseur N, Bohers E, et al. Digital PCR for quantification of recurrent and potentially actionable somatic mutations in circulating free DNA from patients with diffuse large B-cell lymphoma. Leukemia & lymphoma 2016:1-9.
24. Mareschal S, Dubois S, Lecroq T, et al. Rgb: a scriptable genome browser for R. Bioinformatics 2014;30:2204-2205.
25. Li Q, Birkbak NJ, Gyorffy B, et al. Jetset: selecting the optimal microarray probe set to represent a gene. BMC bioinformatics 2011;12:474.
26. Ritchie ME, Phipson B, Wu D, et al. limma powers differential expression analyses for RNA-sequencing and microarray studies. Nucleic acids research 2015.
27. Kau TR, Schroeder F, Ramaswamy S, et al. A chemical genetic screen identifies inhibitors of regulated nuclear export of a Forkhead transcription factor in PTEN-deficient tumor cells. Cancer cell 2003;4:463-476.
28. Cheson BD, Horning SJ, Coiffier B, et al. Report of an international workshop to standardize response criteria for non-Hodgkin's lymphomas. NCI Sponsored International Working Group. Journal of clinical oncology : official journal of the American Society of Clinical Oncology 1999;17:1244.
29. Dong X, Biswas A, Suel KE, et al. Structural basis for leucine-rich nuclear export signal recognition by CRM1. Nature 2009;458:1136-1141.
30. Saunders CT, Baker D. Evaluation of structural and evolutionary contributions to deleterious mutation prediction. Journal of molecular biology 2002;322:891-901.
31. Kircher M, Witten DM, Jain P, et al. A general framework for estimating the relative pathogenicity of human genetic variants. Nature genetics 2014;46:310-315.
32. Joos S, Otano-Joos MI, Ziegler S, et al. Primary mediastinal (thymic) B-cell lymphoma is characterized by gains of chromosomal material including 9p and amplification of the REL gene. Blood 1996;87:1571-1578.
33. Weniger MA, Gesk S, Ehrlich S, et al. Gains of REL in primary mediastinal B-cell lymphoma coincide with nuclear accumulation of REL protein. Genes, chromosomes & cancer 2007;46:406-415.
34. Lenz G, Wright GW, Emre NC, et al. Molecular subtypes of diffuse large B-cell lymphoma arise by distinct genetic pathways. Proceedings of the National Academy of Sciences of the United States of America 2008;105:13520-13525.
35. Reichel J, Chadburn A, Rubinstein PG, et al. Flow sorting and exome sequencing reveal the oncogenome of primary Hodgkin and Reed-Sternberg cells. Blood 2015;125:1061-1072.
36. Aguiar RC, Takeyama K, He C, et al. B-aggressive lymphoma family proteins have unique domains that modulate transcription and exhibit poly(ADP-ribose) polymerase activity. The Journal of biological chemistry 2005;280:33756-33765.
37. Han X, Wang J, Shen Y, et al. CRM1 as a new therapeutic target for non-Hodgkin lymphoma. Leukemia research 2015;39:38-46.
38. Tai YT, Landesman Y, Acharya C, et al. CRM1 inhibition induces tumor cell cytotoxicity and impairs osteoclastogenesis in multiple myeloma: molecular mechanisms and therapeutic implications. Leukemia 2014;28:155-165.
39. Weniger MA, Melzner I, Menz CK, et al. Mutations of the tumor suppressor gene SOCS-1 in classical Hodgkin lymphoma are frequent and associated with nuclear phospho-STAT5 accumulation. Oncogene 2006;25:2679-2684.
40. Ritz O, Guiter C, Castellano F, et al. Recurrent mutations of the STAT6 DNA binding domain in primary mediastinal B-cell lymphoma. Blood 2009;114:1236-1242.

41. Dunleavy K, Grant C, Eberle FC, et al. Gray zone lymphoma: better treated like hodgkin lymphoma or mediastinal large B-cell lymphoma? Current hematologic malignancy reports 2012;7:241-247.
42. Dunleavy K, Wilson WH. Primary mediastinal B-cell lymphoma and mediastinal gray zone lymphoma: do they require a unique therapeutic approach? Blood 2015;125:33-39.
43. Feuerhake F, Kutok JL, Monti S, et al. NFkappaB activity, function, and target-gene signatures in primary mediastinal large B-cell lymphoma and diffuse large B-cell lymphoma subtypes. Blood 2005;106:1392-1399.
44. Yuan J, Wright G, Rosenwald A, et al. Identification of Primary Mediastinal Large B-cell Lymphoma at Nonmediastinal Sites by Gene Expression Profiling. The American journal of surgical pathology 2015;39:1322-1330.
45. Melzner I, Bucur AJ, Bruderlein S, et al. Biallelic mutation of SOCS-1 impairs JAK2 degradation and sustains phospho-JAK2 action in the MedB-1 mediastinal lymphoma line. Blood 2005;105:2535-2542.
46. Marg A, Shan Y, Meyer T, et al. Nucleocytoplasmic shuttling by nucleoporins Nup153 and Nup214 and CRM1-dependent nuclear export control the subcellular distribution of latent Stat1. The Journal of cell biology 2004;165:823-833.
47. Steidl C, Shah SP, Woolcock BW, et al. MHC class II transactivator CIITA is a recurrent gene fusion partner in lymphoid cancers. Nature 2011;471:377-381.
48. Xie L, Ritz O, Leithauser F, et al. FOXO1 downregulation contributes to the oncogenic program of primary mediastinal B-cell lymphoma. Oncotarget 2014;5:5392-5402.
49. Mao L, Yang Y. Targeting the nuclear transport machinery by rational drug design. Current pharmaceutical design 2013;19:2318-2325.
50. Raval A, Weissman JD, Howcroft TK, et al. The GTP-binding domain of class II transactivator regulates its nuclear export. J Immunol 2003;170:922-930.
51. Muqbil I, Kauffman M, Shacham S, et al. Understanding XPO1 target networks using systems biology and mathematical modeling. Current pharmaceutical design 2014;20:56-65.
52. Swameye I, Muller TG, Timmer J, et al. Identification of nucleocytoplasmic cycling as a remote sensor in cellular signaling by databased modeling. Proceedings of the National Academy of Sciences of the United States of America 2003;100:1028-1033.
53. Neggers JE, Vercruysse T, Jacquemyn M, et al. Identifying drug-target selectivity of small-molecule CRM1/XPO1 inhibitors by CRISPR/Cas9 genome editing. Chemistry & biology 2015;22:107-116.
54. Gravina G, Senapedis W, McCauley D, et al. Nucleo-cytoplasmic transport as a therapeutic target of cancer. Journal of hematology & oncology 2014;7:85.
55. Yoshimura M, Ishizawa J, Ruvolo V, et al. Induction of p53-mediated transcription and apoptosis by exportin-1 (XPO1) inhibition in mantle cell lymphoma. Cancer Sci 2014;105:795-801.

Figure legends

Figure 1. Mutations of *XPO1* in lymphoma cases

A. The *XPO1* mutation rate in DLBCL, PMBL, HL and GZL cases. **B.** The E571 XPO1 mutation as illustrated by an electropherogram and IGV view (NM_003400:exon15: c.G1711A; p.E571K; chr2:g.61719**472**C>T). Numbers of reads (y-axis), Nucleotides and corresponding amino-acids (x-axis) are indicated . **C.** The XPO1 domain, which was sequenced by personal genome machine (PGM) (exon 15-18) and the Sanger method (exon 15) is indicated according to the corresponding amino acid numbers. Variants located in exon 15 of DLBCL/PMBL patients are depicted (red arrows). Additional

variants reported in chronic lymphocytic leukemia and esophageal squamous cell carcinoma cases are also depicted (black arrows).

Figure 2. KPT-185 inhibits cell proliferation and induces cell death in PMBL cell lines

A. Western blot of whole-cell protein extracts after 48 hours of incubation in the presence (+) or absence (-) of 2 μM KPT-185. **B.** Viable cells were measured via the MTS assay in the PMBL and Jurkat cell lines after 72 h of treatment with KPT-185 at different doses. The graph shows the inhibition of cell proliferation compared to DMSO-treated cells (mean ± standard deviation of 3 independent experiments). **C**. Cells were labelled with the cell proliferation indicator dye eFluor 670 at day 0 and then incubated for 48 h in the presence or absence of 2 μM KPT-185. The eFluor fluorescence ratio on day 2/day 0 represents the dilution of the dye due to cell division (mean ± standard deviation of 3 independent experiments). **D.** The eFluor fluorescence ratio at day 2 in DMSO-/KPT-185-treated cells was calculated to evaluate cell proliferation upon KPT-185 treatment compared to DMSO treatment (mean ± standard deviation of 3 independent experiments). **E.** The cells were labelled with Annexin V-FITC/propidium iodide after 20 h of incubation in DMSO or 2 μM KPT-185. The plot shows the percentage of Annexin V-positive cells (mean ± standard deviation of 3 independent experiments).

Figure 3. REV-GFP expressing U2OS cells transfected with plasmids encoding XPO1 variants.

The colocalization of XPO1 proteins carrying a red fluorescent tag with REV-RFP (green) in U20S cells was assessed by confocal fluorescence microscopy analysis. REV-GFP (green fluorescent) expressing U2OS cells were transfected with wild type (WT) XPO1-RFP (red fluorescent protein), XPO1-C528S-RFP, XPO1-E571K-mCherry, and XPO1-E571G-mCherry mutants. The pictures show the cells treated with 1μM KPT-330 for 8 hours. **(A)** The REV-GFP localizes in the nucleoli of the cells within the nucleus and its shuttle to the cytoplasm is inhibited by KPT-330; WT XPO1-RFP exhibits a pan-cellular localization (nuclear/nuclear rim and cytoplasmic) **(B)** Co-expression of REV-GFP with XPO1-C528S-RFP results in a colocalization of REV-GFP with XPO1-RFP in the cytoplasm and nuclear rim, independently of KPT-330 action **(C)(D)** Rev-GFP with XPO1-E571K/G-mCherry exhibits a nuclear localization following inhibition of the mutant XPO1 proteins by KPT-330, as shown in panel (A).

	Molecular PMBL cohort				Histological PMBL cohort			
Patients	**Entire cohort**	**wild type XPO1 patients**	**mutated XPO1 patients**	p	**Entire cohort**	**wild type XPO1 patients**	**mutated XPO1 patients**	p
n (%)	**32**	**16**	**16**		**85**	**73**	**12**	
Males	15 (47)	10 (62)	5 (38)	0.15	46 (54)	42 (57)	4 (33)	0.13
Females	17 (53)	6 (38)	11 (62)		39 (46)	31 (43)	8 (67)	
Sex- ratio (M/F)	0.50	0.62	0.41		0.54	0.57	0.33	
Age (years)								
Median	34.5	36	33		37.6	37	34	
Mean	33.8	35	32	0.38	37.6	38	37	0.86
Range	19-56	19-56	19-46		14-74	14-74	19-62	
SD	10.66	10.67	8.64		12.93	13.08	12.5	
Performance status								
0-1	29 (91)	15 (94)	14 (88)	1	79 (93)	60 (82)	10 (83)	1.0
2-4	3 (9)	1 (6)	2 (12)		6 (7)	13 (8)	2 (7)	
Ann Arbor Stage								
0-2	19 (59)	11 (69)	8 (50)	0.47	46 (55)	40 (55)	6 (50	0.76
3-4	13 (41)	5 (31)	8 (50)		39 (45)	33 (45)	6 (50)	
aaIPI								
0-1	20 (62)	11 (69)	9 (56)	0.71	47 (55)	43 (59)	5 (42)	0.35
2-3	12 (38)	5 (31)	7 (44)		38 (45)	30 (41)	7 (58)	
elevated LDH								
No	11 (34)	8 (50)	3 (19)	0.13	17 (31)	16 (22)	1 (8)	0.44
Yes	21 (66)	8 (50)	13 (81)		68 (69)	57 (78)	11 (92)	
Bulky Mass > 10 cm								
No	15 (47)	8 (50)	7 (44)		38 (45)	32 (44)	6 (50)	
Yes	17 (53)	8 (50)	9 (56)	1	46 (55)	40 (56)	6 (50)	0.79
NA	0	0	0		1	1	0	
Treatment								
R-CHOP/R-CHOP like	6 (19)	2 (12)	4 (25)	0.65	40 (47)	27 (36)	6 (50)	0.52
ACVBP/R-ACVBP like	26 (81)	14 (88)	12 (75)		45 (53)	46 (63)	6 (50)	
R containing regimens	15 (47)	8 (50)	7 (43)		76 (89)	65 (89)	11 (92)	
Response rate at the end of initial treatment								
CR/unconfirmed CR	19 (59)	10 (63)	9 (56)		67 (85)	58 (85)	9 (82)	
Partial response/progressive disease	13 (41)	6 (37)	7 (44)	1	12 (15)	10 (15)	2 (18)	0.86
NA	0	0	0		6	5	1	
Relapse/lymphoma progression								
No	20 (62)	12 (75)	8 (50)		68 (81)	58 (80)	10 (83)	
Yes	12 (38)	4 (25)	8 (50)	0.27	16 (19)	14 (20)	2 (7)	1
NA	0	0	0		1	1	0	
Cause of deaths								
n (%)	7 (22)	1 (6)	6 (38)		8 (9)	7 (10)	1 (8)	
lymphoma-related	5	1	4		4	4	0	
toxicity	1	0	1	1	2	1	1	0.5
other cause	1	0	1		2	2	0	

Table 1. Clinical chararecteristics of primary mediastinal patients in molecular and histological-defined groups according to *XPO1* mutational status.

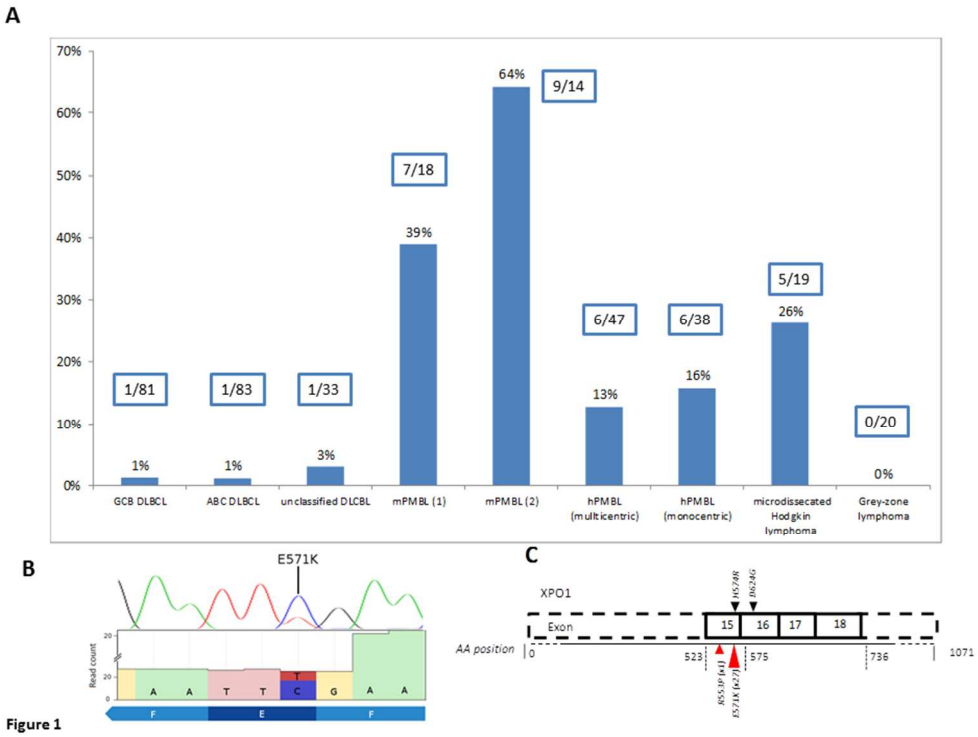

Figure 1

Figure 1. Mutations of XPO1 in lymphoma cases

A. The XPO1 mutation rate in DLBCL, PMBL, HL and GZL cases. B. The E571 XPO1 mutation as illustrated by an electropherogram and IGV view (NM_003400:exon15: c.G1711A; p.E571K; chr2:g.61719472C>T). Numbers of reads (y-axis), Nucleotides and corresponding amino-acids (x-axis) are indicated . C. The XPO1 domain, which was sequenced by personal genome machine (PGM) (exon 15-18) and the Sanger method (exon 15) is indicated according to the corresponding amino acid numbers. Variants located in exon 15 of DLBCL/PMBL patients are depicted (red arrows). Additional variants reported in chronic lymphocytic leukemia and esophageal squamous cell carcinoma cases are also depicted (black arrows).

254x190mm (96 x 96 DPI)

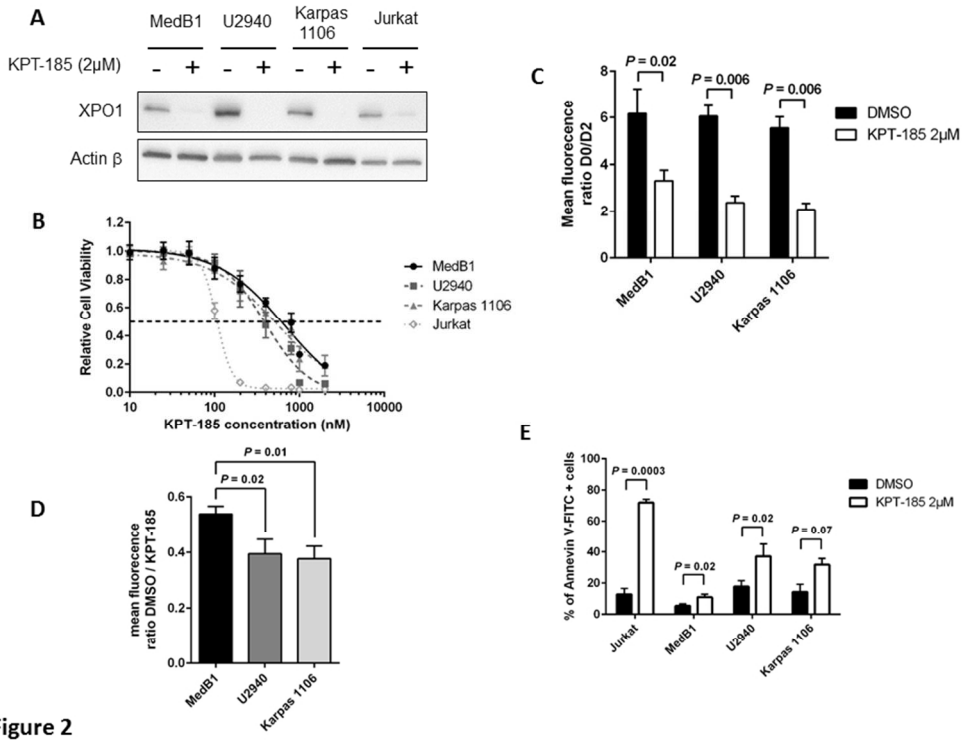

Figure 2

Figure 2. KPT-185 inhibits cell proliferation and induces cell death in PMBL cell lines

A. Western blot of whole-cell protein extracts after 48 hours of incubation in the presence (+) or absence (-) of 2 μM KPT-185. B. Viable cells were measured via the MTS assay in the PMBL and Jurkat cell lines after 72 h of treatment with KPT-185 at different doses. The graph shows the inhibition of cell proliferation compared to DMSO-treated cells (mean ± standard deviation of 3 independent experiments). C. Cells were labelled with the cell proliferation indicator dye eFluor 670 at day 0 and then incubated for 48 h in the presence or absence of 2 μM KPT-185. The eFluor fluorescence ratio on day 2/day 0 represents the dilution of the dye due to cell division (mean ± standard deviation of 3 independent experiments). D. The eFluor fluorescence ratio at day 2 in DMSO-/KPT-185-treated cells was calculated to evaluate cell proliferation upon KPT-185 treatment compared to DMSO treatment (mean ± standard deviation of 3 independent experiments). E. The cells were labelled with Annexin V-FITC/propidium iodide after 20 h of incubation in DMSO or 2 μM KPT-185. The plot shows the percentage of Annexin V-positive cells (mean ± standard deviation of 3 independent experiments).

254x190mm (96 x 96 DPI)

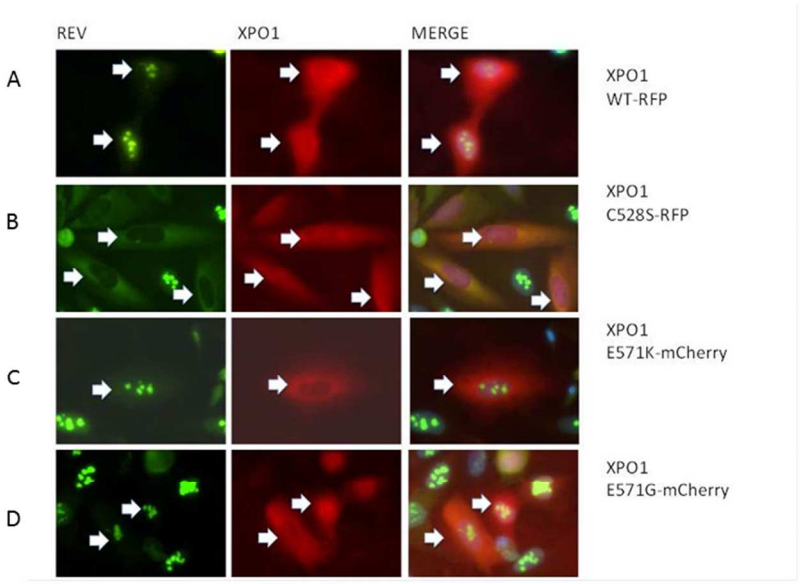

Figure 3

Figure 3. REV-GFP expressing U2OS cells transfected with plasmids encoding XPO1 variants. The colocalization of XPO1 proteins carrying a red fluorescent tag with REV-RFP (green) in U20S cells was assessed by confocal fluorescence microscopy analysis. REV-GFP (green fluorescent) expressing U2OS cells were transfected with wild type (WT) XPO1-RFP (red fluorescent protein), XPO1-C528S-RFP, XPO1-E571K-mCherry, and XPO1-E571G-mCherry mutants. The pictures show the cells treated with 1μM KPT-330 for 8 hours. (A) The REV-GFP localizes in the nucleoli of the cells within the nucleus and its shuttle to the cytoplasm is inhibited by KPT-330; WT XPO1-RFP exhibits a pan-cellular localization (nuclear/nuclear rim and cytoplasmic) (B) Co-expression of REV-GFP with XPO1-C528S-RFP results in a colocalization of REV-GFP with XPO1-RFP in the cytoplasm and nuclear rim, independently of KPT-330 action (C)(D) Rev-GFP with XPO1-E571K/G-mCherry exhibits a nuclear localization following inhibition of the mutant XPO1 proteins by KPT-330, as shown in panel (A).

254x190mm (96 x 96 DPI)